JPE 18-3-17

https://doi.org/10.6113/JPE.2018.18.3.826
ISSN(Print): 1598-2092 / ISSN(Online): 2093-4718

A Simple Real-Time DMPPT Algorithm for PV Systems Operating under Mismatch Conditions

Aniruddha Kamath M.[†], Jayanta Biswas[*], Anjana K. G.[**], and Mukti Barai[**]

[*]Freelance Researcher
[†,**]Department of Electrical Engineering, National Institute of Technology, Calicut, India

Abstract

This paper presents a distributed maximum power point tracking (DMPPT) algorithm based on the reference voltage perturbation (RVP) method for the PV modules of a series PV string. The proposed RVP-DMPPT algorithm is developed to accurately track the maximum power point (MPP) for each PV module operating under all atmospheric conditions with a reduced hardware overhead. To study the influence of parameters such as the controller reference voltage (V_{ref}) and PV current (I_{pv}) on the PV string voltage, a small signal model of a unidirectional differential power processing (DPP) based PV-Bus architecture is developed. The steady state and dynamic performances of the proposed RVP DMPPT algorithm and small signal model of the unidirectional DPP based PV-Bus architecture are demonstrated with simulations and experimental results. The accuracy of the RVP DMPPT algorithm is demonstrated by obtaining a tracking efficiency of 99.4% from the experiment.

Key words: Maximum power point tracking (MPPT), Photovoltaic (PV), Solar energy

I. INTRODUCTION

Solar energy is nonhazardous, freely available, abundant power source that can be easily converted to electrical energy. A number of PV modules are connected in series and many such series strings are connected in parallel to enhance the power capability of a PV system [1]. The PV current and voltage vary significantly due to variations in atmospheric irradiance and temperature. The current generated by a series PV string is significantly limited by the non-uniform illumination of PV modules in the string. The main factors responsible for the non-uniform illumination among PV modules in a string are partial shading, manufacturing defects, aging, etc. [2], [3]. The configuration of a PV string with non-uniform illumination and its corresponding I-V and P-V characteristics are shown in Fig. 1(a) and Fig. 1(b), respectively. In order to extract the maximum power from a PV string operating under non-uniform illumination several methods have been reported [4]-[6]. The solutions reported to operate the PV modules in a string at their respective MPPs under non-uniform illumination include:

- The use of bypass diodes which leads to the bypassing of entire PV modules from a string. This makes the partially shaded PV modules inoperative and introduces multiple peaks in P-V curve of a system [7]-[11].
- Reconfiguration MPPT (RMPPT), where the connections between the PV modules in a system are modified to obtain the best combination to extract the maximum power [12]. The main drawback is the necessity of switches and a relay setup and the periodical disconnection of some PV modules.
- Distributed maximum power point tracking (DMPPT), where the maximum power is extracted from a PV string using dedicated DC-DC converters [13]. The DMPPT method is implemented by two configurations, which are known as full power dedicated DC-DC converter (FPDC) methods [14]-[16] and a DPP with the compensation power dedicated DC-DC converter (CPDC) method.

The dedicated converter used in the FPDC configuration processes the entire PV module power which requires components of higher ratings. The overall efficiency of the FPDC configuration is less due to increased losses in the converter. The overall power conversion efficiency of a PV system is improved by operating dedicated DC-DC converters

Manuscript received May 28,2017; accepted Dec.13, 2017
Recommended for publication by Associate Editor Joung-Hu Park.
[†]Corresponding Author: aniindia@gmail.com
Tel: +91-9633773764 Fax: +91-0495-2287250, Nat'l Inst. Tech.
[*]Dept. of Electrical Engineering, National Institute of Technology India

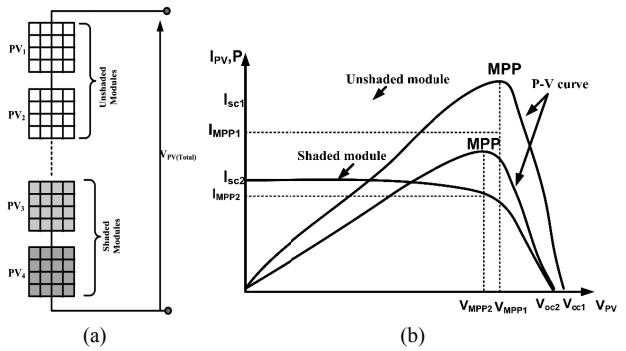

Fig. 1. (a) Series PV string with non-uniform illumination. (b) I-V and P-V characteristics.

only for differential power under non-uniform illumination conditions [17].

Differential power processing (DPP) enables each of the PV modules in a string to operate at its MPP by supplying a small compensation current under non-uniform illumination. The amount of the compensation current depends on the difference between the currents of the most illuminated PV module (MIPVM) in the string and the most shaded PV module [18]-[20]. The dedicated DC-DC converters corresponding to the most illuminated PV modules do not compensate any current while regulating the output voltage of the respective PV module at the MPP. The dedicated converters corresponding to the less illuminated PV modules process only fractional power in order to supply compensation current while regulating the output voltage of the PV module at the MPP. This enables the component ratings for the DPP based DMPPT to be low and the overall efficiency of the configuration to be high. The DPP is generally implemented using three types of configurations with a variety of converter topologies. The configurations are built based on the dedicated converter's connections and communications with the bus. The configurations are known as PV-PV, PV-Virtual Bus and PV-Bus architecture as shown in Fig. 2(a), Fig. 2(b) and Fig. 2(c), respectively. In the PV-PV architecture, differential converters communicate with other PV modules. In the PV-Virtual Bus configuration, differential converters communicate with the virtual bus (an independent energy storage element). Dedicated DC-DC converters communicate with the main bus in the PV-Bus configuration. The differential current under non-uniform illumination conditions is compensated by using various DMPPT algorithms and converter topologies. Current compensation is achieved in [21] and [22], [23] by using a switched capacitor based dedicated converter and a flyback converter based on the DMPPT algorithm. The MPP of each PV module in the string is determined by using separate analog units. Each analog unit consists of a latch, a multiplier and a peak detector circuit. The entire PV string is disconnected from the grid during computation of the MPP. The DMPPT algorithm determines the exact MPP of each PV module. However, this requires extra hardware and an auxiliary supply.

Voltage equalization based DMPPT schemes are presented in [24]-[28]. The string voltage is equally divided by N for N PV modules in a string and individual PV modules are made to operate at that voltage. This method does not guarantee the operation of each PV module at their true MPP. The control complexity also increases with scaled up systems. A duty ratio perturbation based P&O algorithm is used in [29], [30], which requires sensing of the PV current and PV voltage.

In this paper, a reference voltage perturbation (RVP) DMPPT algorithm is proposed to compensate differential currents under non-uniform illumination. The proposed RVP-DMPPT algorithm is implemented on a unidirectional DPP based PV-Bus configuration. Each of the PV modules in a PV string is connected to the output terminals of a converter and the output voltage is regulated by each of the digital controllers by tracking the controller reference voltage. The MPP of each PV module is determined by the proposed RVP-DMPPT algorithm. In this algorithm the reference voltage is perturbed for any change in atmospheric conditions to reach the exact MPP. The PV current is sensed periodically to identify changes in the operating point of a PV module. A change in the PV current indicates a change in the MPP which enables the MPP algorithm to determine a new MPP. This algorithm does not require periodic PV voltage sampling for PV power computation. The PV voltage is obtained from perturbations of the controller reference voltage. The effects of system parameters on the operation of the FPDC based PV array are discussed by developing a small signal model of the system [31]. A linearized small signal model is developed in [32] for the bidirectional DPP based PV-virtual bus architecture. The authors of [32] studied the frequency response of the model for the operation of a PV system in different operating regions. In the literature, various MPP tracking methods have been proposed for the unidirectional DPP based PV-Bus architecture. However, the small signal model of the unidirectional DPP based PV-Bus architecture and analysis are not discussed extensively.

In this paper, a small signal model of the unidirectional DPP based PV-Bus architecture is developed. The effects of parameters such as the controller reference voltage and PV current on the PV string voltage are studied. The steady state and dynamic performances of a system with the proposed RVP-DMPPT algorithm are presented with simulation and experimental results. This paper is organized as follows. Section II presents the DPP based series PV configuration, a description of the proposed RVP-DMPPT algorithm and small signal modeling of the system. Section III describes the design and implementation of the system with simulation and experimental results. The conclusion is presented in section IV.

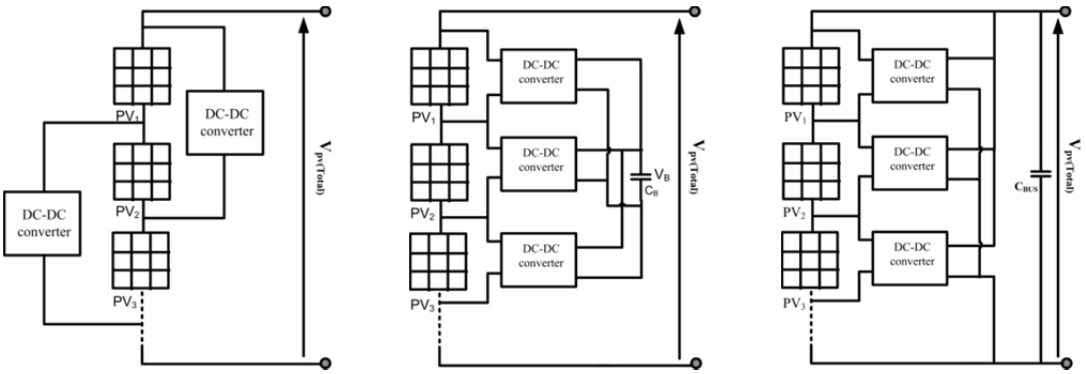

Fig. 2. Types of DPP architectures. (a) PV-PV. (b) PV-Virtual Bus. (c) PV-Bus.

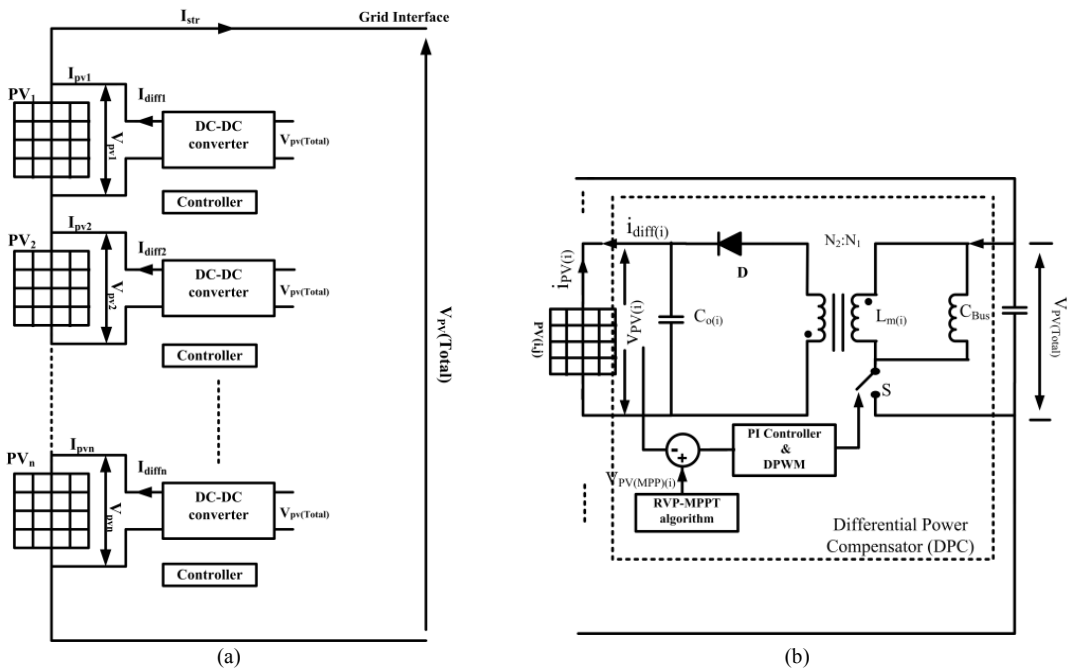

Fig. 3. (a) DPP configuration of a PV string. (b) Single DPP unit.

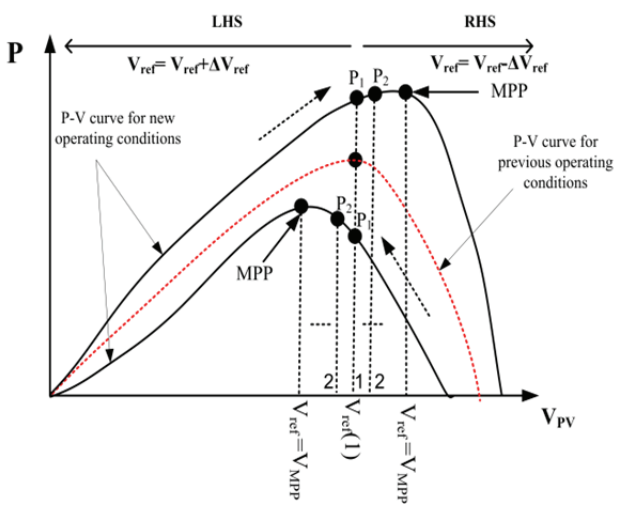

Fig. 4. MPP determination based on the perturbation of V_{ref} on the PV curve.

II. Overview of the Work

A. DPP Based Series Configuration

The main objective of a DPP unit is to supply difference current in order to extract the maximum power from a PV string under non-uniform illumination. The basic functionality of a DPP based series PV configuration is described here. One of the major advantages of DPP is that the converters are required to compensate only for the differential power. This feature of the DPP topology increases the overall system efficiency. The configuration of a PV system with DPP units is shown in Fig. 3(a). The DPP unit consists of a dedicated DC-DC converter with a controller for each of the PV modules in a PV string. The configuration of a DPP unit is shown in Fig. 3(b). Ideally, none of the DPP units needs to compensate under uniform illumination. The DPP unit is only required to process the

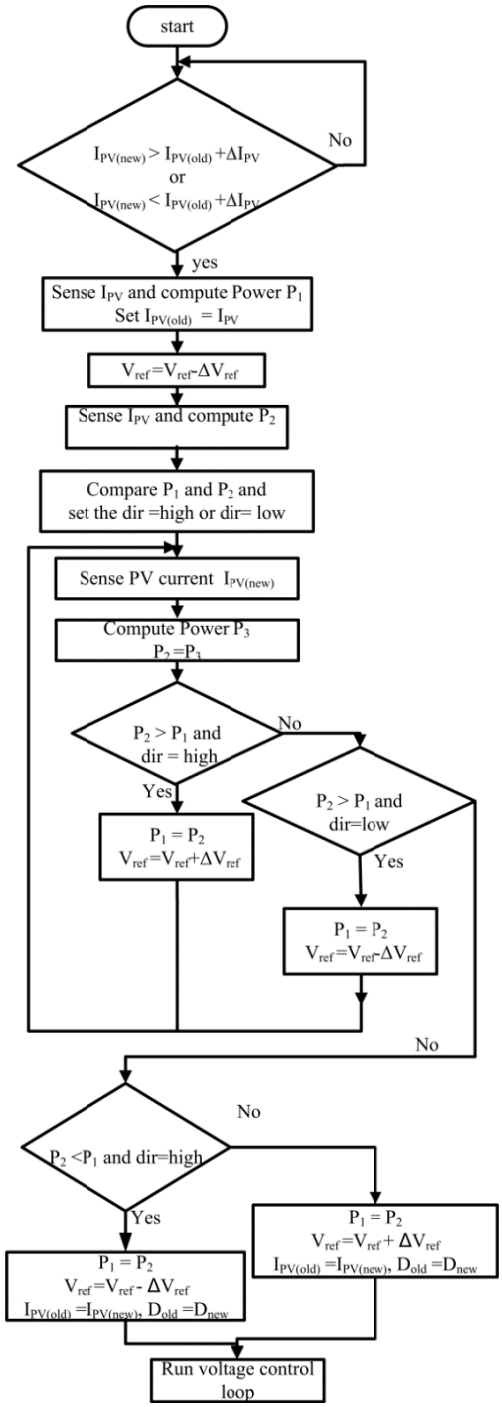

Fig. 5. Flowchart of the RVP-MPPT algorithm.

difference in power (P_{diff}) of a shaded PV module in a PV string by supplying difference current to the string at its MPP. The controller of the DPP unit continuously regulates the output voltage of a PV module at its MPP voltage ($V_{PV(MPP)}$).

The amount of difference current (I_{diff}) for a PV module under non-uniform illumination is determined by the following expression.

$$I_{diff(i)} = I_{string} - I_{PV(i)} \quad (1)$$

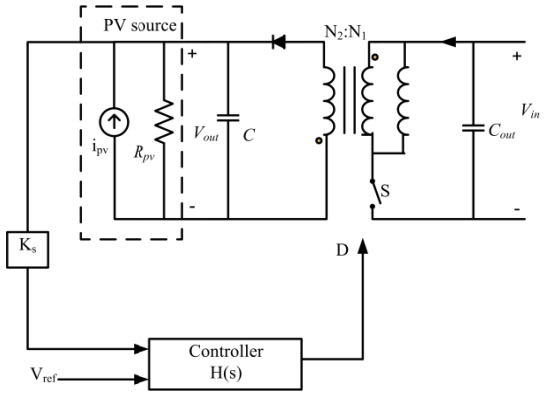

Fig. 6. Simplified model of a PV module and a flyback converter.

where $I_{PV(i)}$ is the current corresponding to a less illuminated PV module. The string current (I_{string}) is equal to the current corresponding to the most illuminated PV module in a PV string. The currents $I_{diff(i)}$, $I_{PV(i)}$ and I_{string} correspond to the secondary side of the DPP units in a PV string. The differential current corresponding to a less illuminated PV module is provided by the grid or auxiliary supply through the primary side of the respective flyback converter. Hence, the difference in power is computed with respect to the primary side of the converters and expressed by the following expression.

$$P_{diff} = V_{PV(Total)}.I_{prim(i)} \quad (2)$$

where P_{diff} is the difference power supplied by the flyback converter of a DPP unit, $V_{PV(Total)}$ is the total PV string voltage, and $I_{prim(i)}$ corresponds to the primary current supplied by the flyback DPP converter.

$$V_{PV(Total)} = \sum_{i=1}^{m} V_{PV(MPP)(i)}$$

$$I_{prim(i)} = \frac{nD_i I_{diff(i)}}{\sqrt{k}}$$

where n is the turns ratio, D_i is the duty ratio, and k is a constant.

$$k = \frac{2L_s}{RT_s} \quad (3)$$

The total difference power ($P_{diff(Total)}$) supplied to the string is:

$$P_{diff(Total)} = V_{PV(Total)}.I_{prim} \quad (4)$$

Where $I_{prim} = \sum_{i=1}^{m} I_{prim(i)}$

The maximum effective power (P_{eff}) extracted from the string is:

$$P_{eff} = V_{PV(Total)} I_{string} - P_{diff(Total)} \quad (5)$$

$$= \sum_{i=1}^{m} V_{PV(MPP)(i)} I_{PV(MPP)(i)} \quad (6)$$

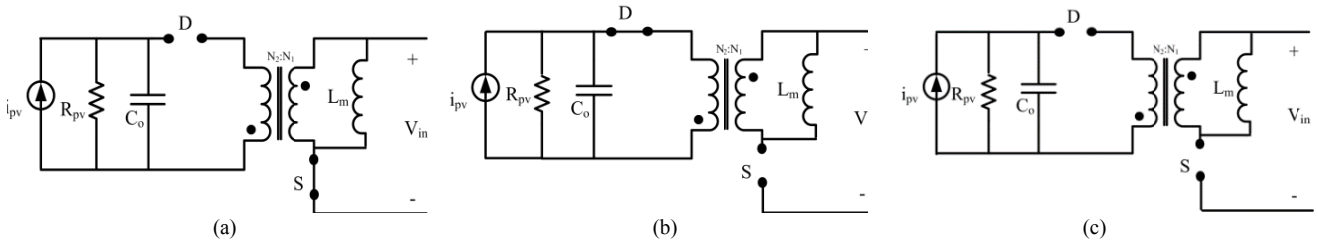

Fig. 7. Equivalent circuits of a converter for three operating intervals. (a) Interval 1. (b) Interval 2. (c) Interval 3.

The maximum power from a PV string can be obtained only when each of the PV modules operates at its MPP. Therefore, the determination of the MPP of PV modules becomes important. A simple reference voltage perturbation DMPPT algorithm (RVP-DMPPT) is presented in the next section.

B. RVP-DMPPT Algorithm

A DMPPT algorithm regulates the output voltage of each PV module at its MPP by regulating the output voltage of the dedicated converter of a DPP unit. In this paper, the MPP of a PV module is determined based on the controller reference voltage (V_{ref}) perturbation method. This is done by setting the controller reference voltage (V_{ref}) at the MPP voltage of the respective PV module ($V_{PV(MPP)}$). The DMPPT algorithm determines the new V_{ref} corresponding to the exact MPP by running the MPPT algorithm at regular intervals. It is assumed that the operating point of the PV module does not change due to atmospheric changes during the process of MPP determination. The change in the operating point on the P-V curve is created with the reference voltage (V_{ref}) perturbation to find a new MPP. The algorithm runs on the controller of each DPP unit. The PV module current is sensed to compute the power at each perturbation to observe the direction of the movement of the operating point. The direction of the movement of the operating point corresponding to the computed power determines the direction of the perturbation of V_{ref} on the P-V curve.

The determination of the MPP process starts based on the location of the computed power (P) and the direction of the movement of P on the P-V curve of a PV module. The power (P_1) is computed at instant 1 based on V_{ref} and $I_{PV(1)}$, which correspond to the previous MPP. V_{ref} is decremented by ΔV_{ref} and P_2 is computed with the current ($I_{PV(2)}$) sensed at instant 2 as shown in Fig. 4. The expressions of P_1 and P_2 are given below.

$$P_1 = V_{ref} * I_{PV(1)} \tag{7}$$

$$P_2 = (V_{ref} - \Delta V_{ref}) * I_{PV(2)} \tag{8}$$

P_1 and P_2 are compared. The location of the new operating point is determined either on left hand side (LHS) or the right hand side (RHS) with respect to the MPP based on $P_2 < P_1$ or $P_2 > P_1$ of the new P-V curve. The variable dir is set to low or high based on the location of the operating point on the LHS or RHS, respectively. V_{ref} is continuously incremented or decremented when dir is low or high until the MPP is reached. The continuous comparison of P_2 and P_1, with the value held by the dir variable is presented by (9) and (10).

$$V_{ref} = V_{ref} + \Delta V_{ref} \; if \; P_2 > P_1 \; with \; dir = high \tag{9}$$

$$V_{ref} = V_{ref} - \Delta V_{ref} \; if \; P_2 > P_1 \; with \; dir = low \tag{10}$$

The condition $P_2 < P_1$, suggests that the MPP is crossed and the MPP is determined at the previous instant (P_1). The V_{ref} corresponding to P_1 is a new MPP and serves as a new V_{ref} for the controller. The PI controller regulates the output voltage of the converter at a new V_{ref} ($V_{PV(MPP)}$). A flowchart of the algorithm is presented in Fig. 5.

C. Modeling of the System

A small signal model of the DPP unit in a PV string is developed in this section to study the dynamic behavior. A linearized averaged model of the DPP unit is shown in Fig. 6. The PV module is modeled as a constant current source (i_{pv}) with a variable resistance (R_{pv}). The state variables of the DPP unit are the inductor current ($i_L(t)$) and capacitor voltage($v_C(t)$) of the flyback converter. The input variables are the total PV voltage ($v_{in}(t)$) and the PV current ($i_{pv}(t)$). The control variable is the duty ratio of the flyback converter (D).

The analysis of the small signal modeling for the DPP unit is described based upon small perturbations of the variables about an operating point [33]. The variables are expressed as follows.

$$i_L(t) = I_L + \hat{i}_L \;\; ; \;\; v_C(t) = V_C + \hat{v}_C \;\; ; \;\; i_{pv}(t) = I_{pv} + \hat{i}_{pv} \;\; ;$$

$$v_{in}(t) = V_{in} + \hat{v}_{in} \; ; \; D(t) = D + \hat{d}$$

The flyback converter in the DPP unit operates in the discontinuous conduction mode (DCM). The structures of the equivalent circuit under different operating intervals of the flyback converter in the DCM are shown in Fig. 7(a), Fig. 7(b) and Fig. 7(c). The expressions of the state variables for the three equivalent circuits of the converter are presented in the state space form for three operating intervals. In interval 1, when the switch S is on and the diode D is off, the state space equations corresponding to Fig. 7(a) are described by (11).

$$\begin{bmatrix} \dot{i}_L \\ \dot{v}_C \end{bmatrix} = \begin{bmatrix} 0 & 0 \\ 0 & \frac{-1}{R_{pv}C} \end{bmatrix} \begin{bmatrix} i_L \\ v_C \end{bmatrix} + \begin{bmatrix} \frac{1}{L_m} & 0 \\ 0 & \frac{1}{C} \end{bmatrix} \begin{bmatrix} v_{in} \\ i_{pv} \end{bmatrix} \quad (11)$$

Similarly, during interval 2, when the switch S is off and the diode D is on, the state space equations corresponding to Fig. 7(b) are described by (12).

$$\begin{bmatrix} \dot{i}_L \\ \dot{v}_C \end{bmatrix} = \begin{bmatrix} 0 & \frac{1}{L_m} \\ \frac{-1}{C} & \frac{-1}{R_{pv}C} \end{bmatrix} \begin{bmatrix} i_L \\ v_C \end{bmatrix} + \begin{bmatrix} 0 & 0 \\ 0 & \frac{1}{C} \end{bmatrix} \begin{bmatrix} v_{in} \\ i_{pv} \end{bmatrix} \quad (12)$$

The state space equations during interval 3 when both the switch S and the diode D are off, corresponding to Fig. 7(c), are described by (13).

$$\begin{bmatrix} \dot{i}_L \\ \dot{v}_C \end{bmatrix} = \begin{bmatrix} 0 & 0 \\ 0 & \frac{-1}{R_{pv}C} \end{bmatrix} \begin{bmatrix} i_L \\ v_C \end{bmatrix} + \begin{bmatrix} 0 & 0 \\ 0 & \frac{1}{C} \end{bmatrix} \begin{bmatrix} v_{in} \\ i_{pv} \end{bmatrix} \quad (13)$$

In order to derive an averaged model of the system, the equations of all three intervals are averaged over a switching cycle.

$$A = \begin{bmatrix} 0 & \frac{D_2}{L_m} \\ \frac{-D_2}{L_m} & \frac{-1}{R_{pv}C} \end{bmatrix} \quad (14)$$

$$B = \begin{bmatrix} \frac{D_1}{L_m} & 0 \\ 0 & \frac{1}{C} \end{bmatrix} \quad (15)$$

The small signal model of the converter is obtained by:

$$\dot{\hat{x}} = A\hat{x} + B\hat{u} + f_1\hat{d}_1 + g_1\hat{d}_2 \quad (16)$$

where:

$$f_1 = (A_1 - A_3)X_1 + (B_1 - B_3)V_{in} \quad (17)$$

$$g_1 = (A_2 - A_3)X_1 + (B_2 - B_3)V_{in} \quad (18)$$

where:

$$X_1 = -A^{-1}BV_{in}$$

The transfer functions of interest are:

The transfer function between the output voltage and the duty ratio.

$$G_{vo\_d} = \frac{\hat{v_o}(s)}{\hat{d}(s)} = \frac{V_{in}}{\sqrt{k}} \left(\frac{1}{1 + \frac{sR_{pv}C}{2}} \right) \quad (19)$$

The transfer function between the output voltage and the input voltage.

$$G_{vo\_vin} = \frac{\hat{v_o}(s)}{\hat{v_{in}}(s)} = M_v \left(\frac{1}{1 + \frac{sR_{pv}C}{2}} \right) \quad (20)$$

where $M_v = \frac{V_o}{V_{in}}$

The transfer function between the output voltage and the PV current G_{vo_ipv}.

$$f_2 = (A_1 - A_3)X_2 + (B_1 - B_3)I_{pv} \quad (21)$$

$$g_2 = (A_2 - A_3)X_2 + (B_2 - B_3)I_{pv} \quad (22)$$

where:

$$X_2 = -A^{-1}BI_{pv}$$

The transfer function between the output voltage and the PV current.

$$G_{vo\_ipv} = \frac{\hat{v_o}(s)}{\hat{i_{pv}}(s)} = \frac{D_1^2}{M_v L_m C} \left(\frac{1}{s^2 + \frac{s}{R_{pv}C} + \frac{D_1^2}{M_v^2 L_m C}} \right) \quad (23)$$

The closed loop transfer function between the output voltage and the reference voltage (V_{ref}).

$$G_{vo\_vref} = \frac{\hat{v_o}(s)}{\hat{v_{ref}}(s)} = \frac{H(s)G_{vo\_d}(s)}{1 + K_s H(s)G_{vo\_d}(s)} \quad (24)$$

$$G_{vo\_vref} = \frac{2V_{in}K_p}{\sqrt{k}R_{pv}CT_p} \left(\frac{(1 + sT_p)}{s^2 + \frac{s}{R_{pv}C} + \frac{2V_{in}K_p}{R_{pv}C\sqrt{k}} + \frac{2V_{in}K_p}{R_{pv}C\sqrt{k}T_p}} \right) \quad (25)$$

where:

$$H(s) = \frac{K_p(1 + sT_p)}{sT_p} \quad (26)$$

where H(s) represents a PI controller, and K_s is the output voltage sensor gain.

$$T_p = \frac{K_p}{K_i}$$

where K_p is the proportional gain, and K_i is the integral gain of the controller.

In order to form a string of PV modules, the converters are connected in the input parallel-output series (IPOS) configuration. A block diagram of the configuration for two converters is shown in Fig. 4. The state space matrices of the IPOS configuration with PV modules is given by:

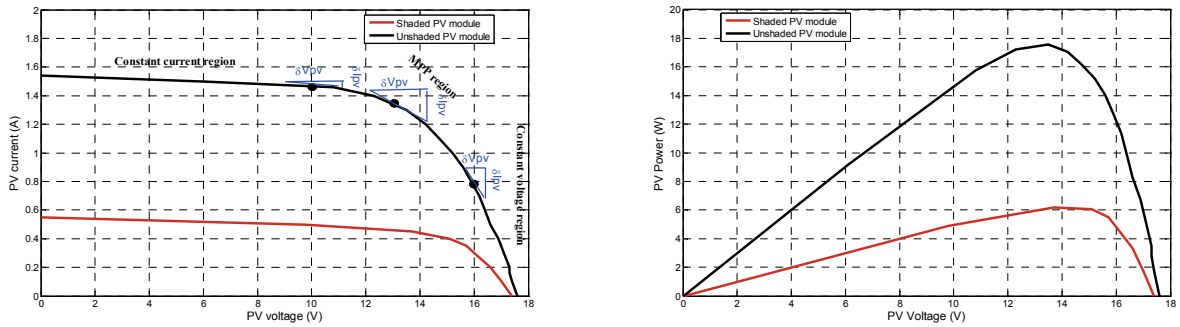

(a) (b)

Fig. 8. (a) I-V characteristic of a PV module and the computation of R_{pv}. (b) Power-voltage characteristics (experimental).

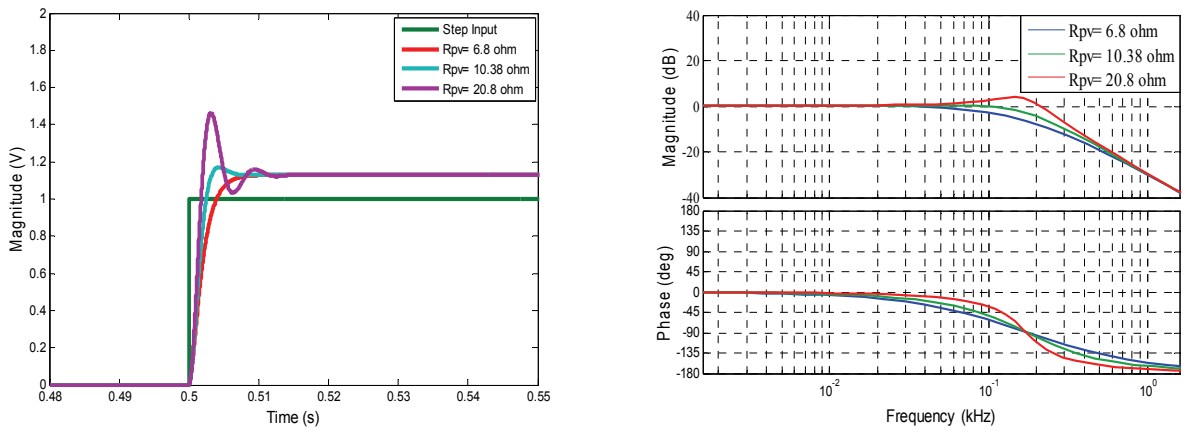

(a) (b)

Fig. 9. (a) Step response of G_{vref_ipv}. (b) Frequency response of G_{vref_ipv}.

$$\dot{\hat{x}} = A\hat{x} + B_v\hat{u}_1 + B_{pv}\hat{u}_2 \tag{27}$$

where:

$$A = \begin{bmatrix} 0 & 0 & \frac{D_{12}}{L_m} & 0 \\ 0 & 0 & 0 & \frac{D_{12}}{L_m} \\ \frac{D_{12}}{C} & 0 & \frac{-1}{R_{pv}C} & \frac{-1}{R_{pv}C} \\ 0 & \frac{D_{22}}{C} & \frac{-1}{R_{pv}C} & \frac{-1}{R_{pv}C} \end{bmatrix} \tag{28}$$

$$B_v = \begin{bmatrix} \frac{D_{11}}{L_m} \\ \frac{D_{21}}{L_m} \\ 0 \\ 0 \end{bmatrix} \tag{29}$$

$$B_{pv} = \begin{bmatrix} 0 & 0 \\ 0 & 0 \\ \frac{1}{C} & 0 \\ 0 & \frac{1}{C} \end{bmatrix} \tag{30}$$

$$C = \begin{bmatrix} 0 & 0 & 1 & 1 \end{bmatrix} \tag{31}$$

where D_{11}, D_{21} and D_{12}, D_{22} are the turn on and turn off duty ratios of flyback converter1 and flyback converter2, respectively.

The transfer functions of interest corresponding to the total output voltage of the PV string are:

$$G_{voT\_vref1}(s) = \frac{\hat{v}_{oT}(s)}{\hat{v}_{ref1}(s)} \tag{32}$$

$$G_{voT\_vref2}(s) = \frac{\hat{v}_{oT}(s)}{\hat{v}_{ref2}(s)} \tag{33}$$

The total output voltage of the PV string $v_{oT}(s)$ is the sum of the output voltages of two DPP units $v_{o1}(s)$ and $v_{o2}(s)$.

$$v_{oT}(s) = v_{o1}(s) + v_{o2}(s) \tag{34}$$

The dynamic expression of the PV string voltage due to a change in the reference voltage in one of the DPP units can be written as follows:

$$\frac{\hat{v}_{oT}(s)}{\hat{v}_{ref1}(s)} = \frac{\hat{v}_{o1}(s)}{\hat{v}_{ref1}(s)} + \frac{\hat{v}_{o2}(s)}{\hat{v}_{ref1}(s)} \tag{35}$$

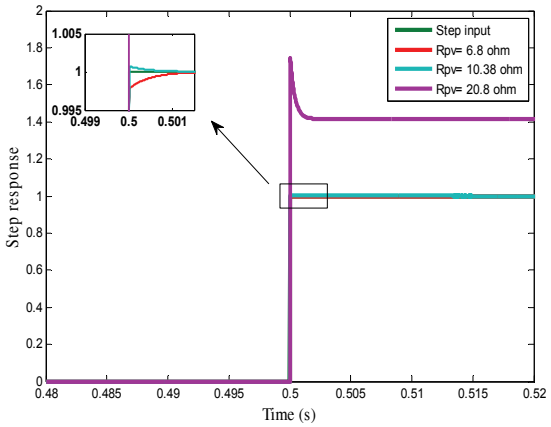

(a)

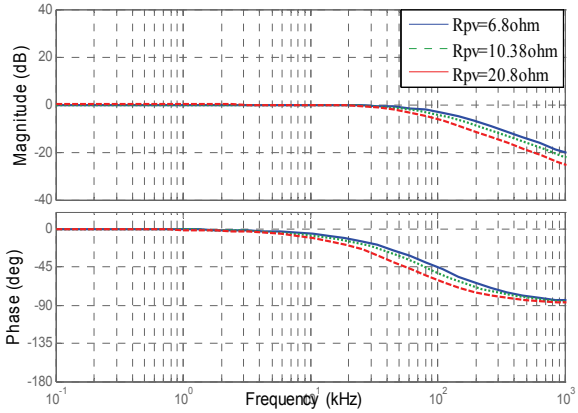

(b)

Fig. 10. (a) Step response of G_{vo_vref}. (b) Frequency response of G_{vo_vref}.

$$\frac{\hat{v}_{oT}(s)}{\hat{v}_{ref2}(s)} = \frac{\hat{v}_{o1}(s)}{\hat{v}_{ref2}(s)} + \frac{\hat{v}_{o2}(s)}{\hat{v}_{ref2}(s)} \tag{36}$$

A change in the reference voltage in each DPP unit occurs only when there is a MPP change in the respective PV module. Therefore, the following terms in the above expressions are considered to be zero.

$$\frac{\hat{v}_{o2}(s)}{\hat{v}_{ref1}(s)} = 0 \quad and \quad \frac{\hat{v}_{o1}(s)}{\hat{v}_{ref2}(s)} = 0$$

$$\frac{\hat{v}_{oT}(s)}{\hat{v}_{ref1}(s)} = \frac{\hat{v}_{o1}(s)}{\hat{v}_{ref1}(s)} \tag{37}$$

$$\frac{\hat{v}_{oT}(s)}{\hat{v}_{ref2}(s)} = \frac{\hat{v}_{o1}(s)}{\hat{v}_{ref2}(s)} \tag{38}$$

The dynamic behavior of the DPP unit is studied based on the step and frequency response of various transfer functions for the three operating regions of a PV module. A PV module is modeled as a constant current source (I_{pv}) with a parallel resistance (R_{pv}) as shown in Fig. 6. The resistance R_{pv} varies with the operating point of the PV module. The determination of R_{pv} with respect certain operating points on the I-V characteristics is shown in Fig. 8(a). Fig. 8(b) shows the P-V characteristics of the same PV module. R_{pv} varies with different operating regions on the V-I characteristics. They are called the constant current, constant voltage and MPP regions, respectively. The value of R_{pv} is computed from the I-V characteristics of the PV module at a certain operating point by linearization as shown in Fig. 8(a). To determine R_{pv}, a tangent is drawn at the operating point and its slope is computed. Different values of R_{pv} obtained from the PV module in the three regions are listed in Table I.

R_{pv} is calculated by:

$$R_{pv} = \frac{\delta V_{pv}}{\delta I_{pv}}$$

TABLE I
EXPERIMENTALLY OBTAINED MODEL PARAMETERS

Parameter	Constant current region	MPP Region	Constant voltage region
V_{pv}(V)	10	13.5	16
R_{pv}(Ω)	20.8	10.38	6.8

δV_{pv} and δI_{pv} are the values of the PV voltage and PV current at certain operating point on the linearized I-V characteristics, respectively.

The step responses of the reference voltage for a step change in the PV module current (G_{vref_ipv}) for different values of R_{pv} are shown in Fig. 9(a). It is observed that the reference voltage tracks the change in the PV current linearly for different values of R_{pv}. The response shows that in the MPP region it varies with moderate response time. Meanwhile, it responds with comparatively faster and slower response times for R_{pv}= 6.8Ω (constant voltage region) and R_{pv}=20.8Ω (constant current region), respectively. The step response and frequency response of the output voltage of the PV module to the reference voltage of the DPP unit (G_{vo_vref}) are shown in Fig. 10(a) and Fig. 10(b), respectively. It is observed that the output voltage of the PV module tracks the change in V_{ref} with a first order response in the MPP and constant voltage regions, respectively. Meanwhile, the output voltage of the PV module responds with a peak value in the constant current region. These studies provide the basis for identifying the MPP of the PV module quickly by preventing the operating point of the PV module from moving away from the MPP region under varying atmospheric conditions.

D. Voltage Mode Controller Design

The control of the output transfer function of each DPP unit in the continuous time domain is derived and given in (19). The discrete domain transfer functions of the flyback converter and the PI controller are obtained by the backward Euler transformation method as follows:

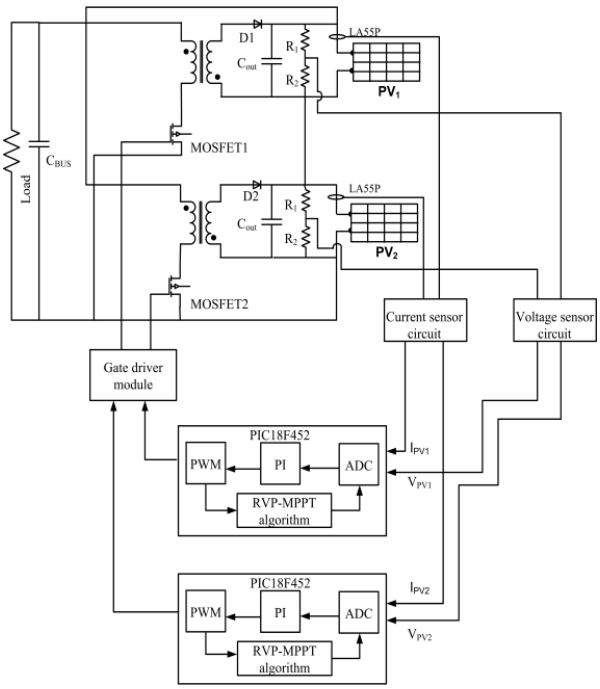

Fig. 11. Schematic of the experimental prototype.

$$s = \frac{(1 - z^{-1})}{T_s}$$

The PI controller transfer function is:

$$\frac{d(z)}{e(z)} = \frac{K_p(1 - z^{-1}) + K_i T_s}{(1 - z^{-1})} \tag{39}$$

where K_p is the proportional gain, and K_i is the integral gain. The flyback converter transfer function is:

$$\frac{V_o(z)}{d(z)} = \frac{V_{in}}{\sqrt{k}} \left(\frac{1}{1 + \frac{(1 - z^{-1})R_{pv}C}{2T_s}} \right) \tag{40}$$

By pole zero matching:

$$K_p = \frac{\sqrt{k} R_{pv} C}{2T_s} \quad , K_i = \frac{\sqrt{k}}{T_s}$$

The PI controller in its discrete time domain is expressed as:

$$d[n] = d[n-1] + ae[n] + be[n-1] \tag{41}$$

where $a = K_p + K_i T_s$, $b = K_p$. Where the constants a and b are functions of K_i and K_p. Both of the flyback converters connected in the string are controlled independently using two separate PI controllers.

III. Experimental Setup and Results

An experimental setup of the DPP based series PV configuration was developed with two PV modules for a PV string. The proposed RVP-DMPPT algorithm was implemented on an 8 bit PIC microcontroller (PIC18F452) along with voltage mode control. The functionality of the DPP units and the RVP-DMPPT algorithm are verified with simulation and experimental results. A schematic of the experimental setup is shown in Fig. 11. The design specifications for the DPP units are listed in Table II and Table III. Table II presents the specifications for each of the PV modules [34]. The design values for the flyback DC-DC converter are listed in Table III. The closed loop operation of the DPP units and the performance of the algorithm are demonstrated in the next section.

TABLE II
PV Module Specifications

Under standard testing conditions (1000W/m^2,25^{o}C) [34]	
Parameter	**Specification**
Nominal power (P)	45W
Open circuit voltage(V_{oc})	21.6V
Short circuit current(I_{sc})	2.85A
Voltageat max. Power ($V_{pv(MPP)}$)	17.7V
Current at max. Power ($I_{pv(MPP)}$)	2.54A

TABLE III
Flyback Converter Design Specifications

Parameter/Component	**Specification**
Input Voltage	20V-36V
Output Voltage	10V-17V (corresponding to MPP)
Switching Frequency	5kHz
Power	30W
MOSFET	IRFP150
Diode	MUR460
Inductance	1mH
Capacitor	100uF

A. Experimental Results

1) Performance of the Flyback Converter

The closed loop performance of the flyback converter of the DPP unit is illustrated with step changes in the controller reference voltage (V_{ref}) and load transient. Fig. 12(a) and Fig. 12(b) show simulation and experimental results of the output voltage for a step change in V_{ref}. It is observed that the converter output voltage reaches the new steady state values in 8ms and 7ms for step changes of 5V up and down, respectively. The load transient response of the converter is shown in Fig. 13. Fig. 13(a) and Fig. 13(b) presents simulation and experimental results of the output voltage of the converter for a load transient of 100% to 60% and 60% to 100%, respectively. It is observed that the converter output voltage remains constant with a minimum deviation from the steady state value. Therefore, it can be concluded that the controller designed for the flyback converter operates satisfactorily.

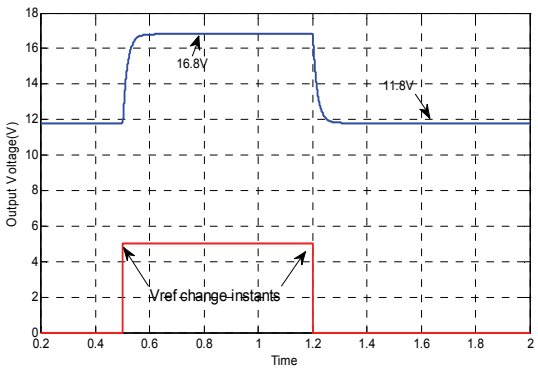

(a)

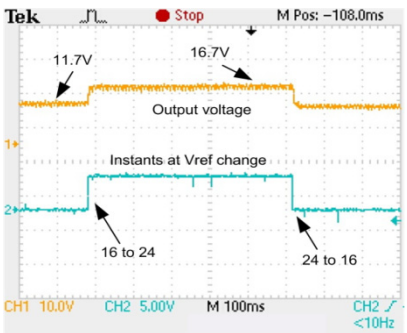

(b)

Fig. 12. Controller set point voltage dynamics (step change in V_{ref}). (a) Simulation. (b) Experimental.

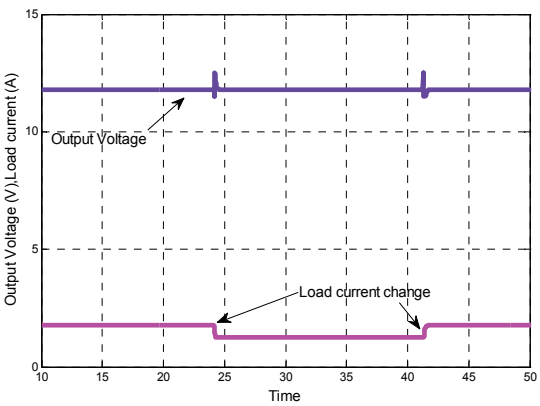

(a)

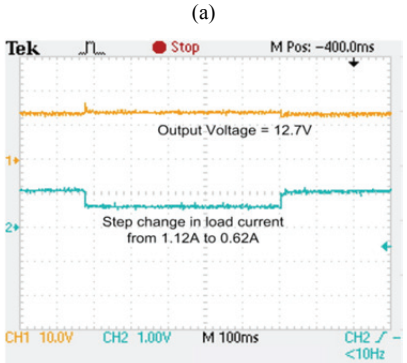

(b)

Fig. 13. Load current dynamics of a flyback converter. (a) Simulation results. (b) Experimental results.

The DPP configuration is built by connecting the inputs of two flyback converters in parallel and the outputs in series (input parallel-output series) of the DPP units. Each PV module is connected across the output of each flyback converter. The operation of the flyback converters are initially tested in a DPP configuration by disconnecting the PV modules. Experimental results corresponding to a change in V_{ref} and load transients are shown in Fig. 14(a) and Fig. 14(b), respectively. It is observed that the total output voltage of the DPP configuration changes due to a step change in the reference voltage in one of the flyback converters. The time taken for the total output voltage to reach the new steady state value is 8ms for a step change of 5V. The dynamics of the total output voltage during a load transient is shown in Fig. 14(b). It is observed that the total output voltage does not deviate from its steady state value. The efficiency of the two flyback converters are measured as 96.17% and 96.8% respectively.

2) Functionality of DPP Units and RVP-DMPPT Algorithm

The operation of the DPP unit along with the RVP-DMPPT algorithm is presented here. The objective of the controller of the flyback converter is to regulate the output voltage of the PV module at its MPP. The reference voltage of the controller is set at the MPP voltage of the PV module. The non-zero output of the controller represents variation in the MPP of the PV module. Therefore, the RVP-DMPPT algorithm is activated to determine the new MPP for the non-zero controller output. The operation of the DPP is tested for a wide range (range of MPPs of the PV module) of digital reference values of V_{ref}. The corresponding analog steady state output voltages are obtained and presented in Fig. 15. It is observed that the controller provides output over a range of 9.6V to 17.6V, which corresponds to the MPP range of the PV module.

The PV modules are connected to the DPP configuration to demonstrate the operation of the DPP and the proposed RVP-DMPPT algorithm. The PV modules are artificially shaded to illustrate the performance of the system under non-uniform illumination. Experimental waveforms of the PV voltages, PV currents, string voltage, duty ratios of the converters and compensation currents of the two converters under two different partial shadings are depicted Fig. 16 and Fig. 17, respectively. Fig. 16 shows the case where PV_1 is unshaded and PV_2 is partially shaded. Fig. 17 shows the case where PV_2 is unshaded and PV_1 is partially shaded. The functionality of the proposed RVP-DMPPT algorithm under the two different partial shadings are illustrated in Fig. 16(a) and Fig. 17(a), respectively. It is observed that the algorithm determines the exact MPP for the PV modules.

The differential current compensation for the shaded PV module under the above two conditions are depicted in Fig. 16(b) and Fig. 17(b), respectively. It is observed that the duty ratios of the flyback converter corresponding to the unshaded

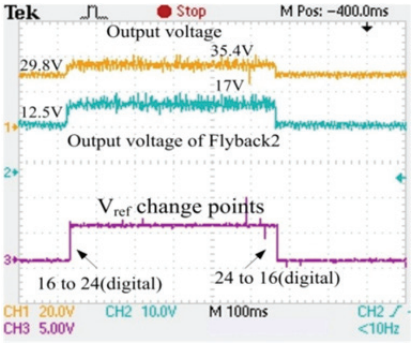

(a)

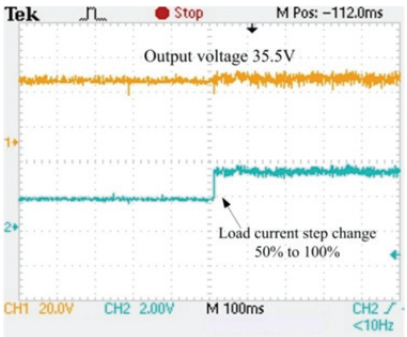

(b)

Fig. 14. Flyback converter IPOS configuration dynamics. (a) Reference voltage step change dynamics. (b) Load current dynamics.

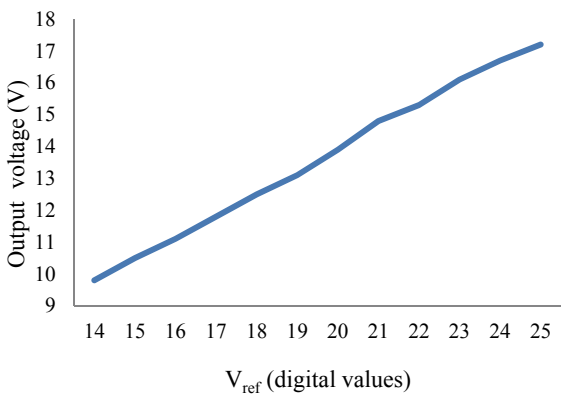

Fig. 15. Variation of the output voltage with controller set point digital values (V_{ref}) (Experimental).

PV module in each case (Fig. 16(b) and Fig. 17(b)) are a lot less. The duty ratios of the flyback converter corresponding to the shaded PV module in each case are higher. This is because an unshaded PV module requires negligible compensation current whereas shaded PV modules are required to inject compensation current into the string. It is observed that the compensation current is injected into the string during the OFF period of the main switch and the ON period of the diode in the secondary of the flyback converter connected to the shaded PV module in each case. The diode current waveforms verify the injection of the compensation current and the DCM operation of each flyback converter.

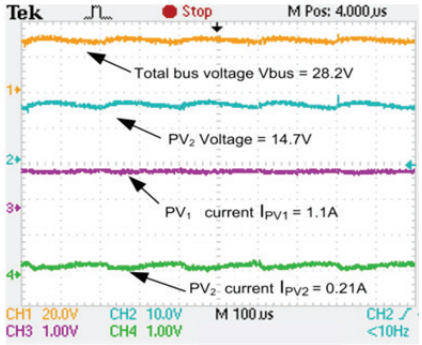

(a)

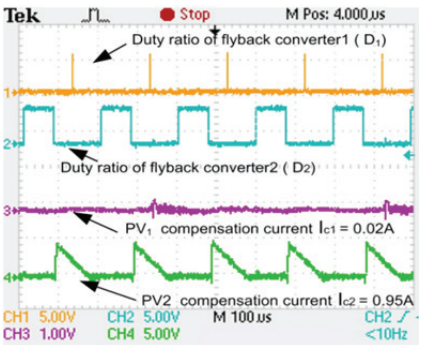

(b)

Fig. 16. DPP unit waveforms (Case1: PV_1 unshaded and PV_2 shaded): (a) Bus voltage (Ch1), PV_2 MPP voltage (Ch2), PV MPP currents (Ch1 and Ch2)); (b) Duty ratios of the converters (Ch1 and Ch2), compensation currents (Ch3 and Ch4).

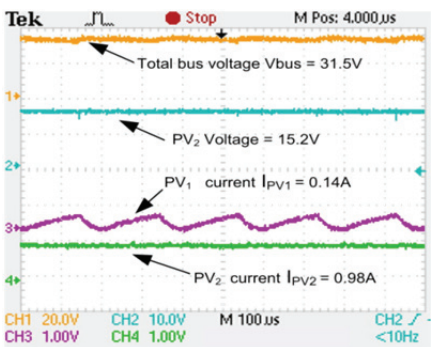

(a)

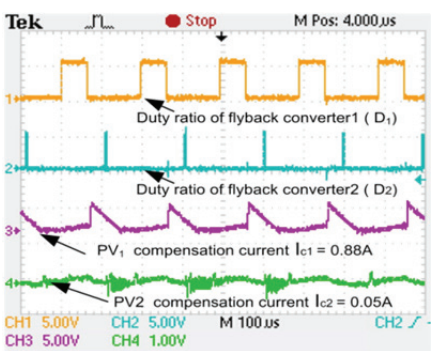

(b)

Fig. 17. DPP unit waveforms (Case2: PV_2 unshaded and PV_1 shaded): (a) Bus voltage (Ch1), PV_2 MPP voltage (Ch2), PV MPP currents (Ch1 and Ch2)); (b) Duty ratios of the converters (Ch1 and Ch2), compensation currents (Ch3 and Ch4).

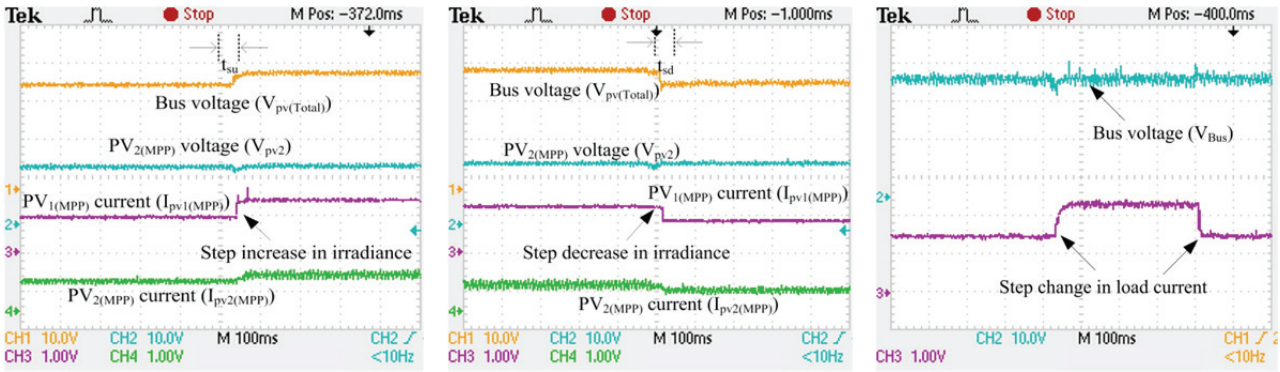

(a) (b) (c)

Fig. 18. Dynamic response for: (a) Step increase in irradiance; (b) Step decrease in irradiance; (c) Step change in the load.

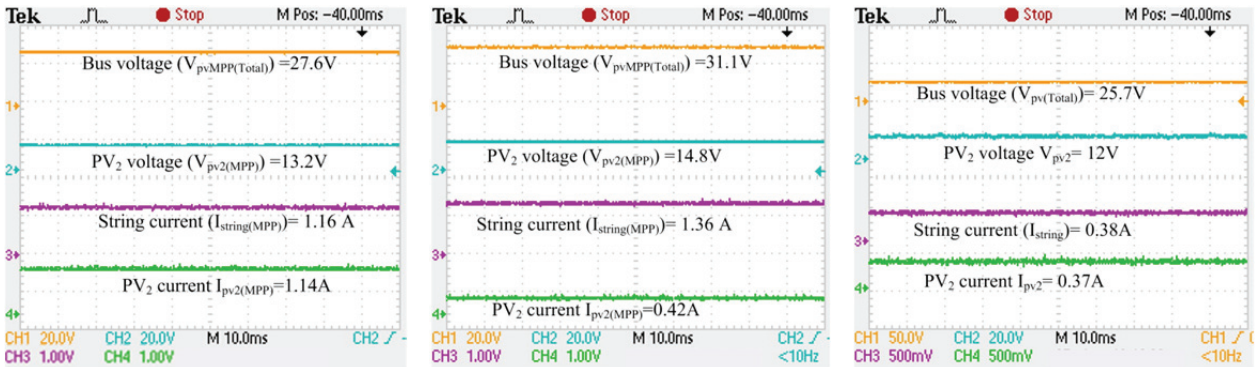

(a) (b) (c)

Fig. 19. DPP Waveforms to show effects of a fault: (a) PV string under uniform illumination (normal operation); (b) PV_1 unshaded, PV_2 shaded (normal operation); (c) PV_1 unshaded, PV_2 shaded (converter corresponding to the PV_2 fault condition).

TABLE IV
COMPARISON OF POWER EXTRACTION

Case	Power (Without DPP units) (W)	Power (With DPP units) (W)
PV1 Shaded PV2 Unshaded	8.4	31.02
PV2 Shaded PV1 Unshaded	7.87	30.24

3) Dynamic Performance

The dynamic performance of the DPP units and the proposed RVP-DMPPT algorithm are illustrated in Fig. 18(a), Fig. 18(b) and Fig. 18(c) based on changes in the irradiance and load. To observe the transient behavior of the RVP-DMPPT algorithm, the irradiance of the PV_2 module of the PV string is artificially step changed by 50%. The corresponding change in the string voltage and the PV currents are shown in Fig. 18(a) and Fig. 18(b) due to changes in irradiance, respectively. It is observed that the proposed algorithm finds the new MPP of the PV_2 module and that the DPP unit performs accordingly to reach the new steady state condition. The tracking time of the proposed algorithm is computed based on the total time taken from the instant of the transient to reach the steady state. This includes the time taken to compute the new MPP and to update the V_{ref} corresponding to the new MPP. The tracking times during a step increase (t_{su}) and during a step decrease (t_{sd}) of irradiance are 25ms and 40ms, respectively.

The dynamic response of the DPP unit for a step change in the load is shown in Fig. 18(c). The string current is changed from 1.4A to 2.2A and from 2.2A to 1.4A to demonstrate the dynamic behavior of the DPP unit and the proposed RVP-DMPPT algorithm. It is observed that the string voltage maintains the total voltage corresponding to the summation of the MPPs of each PV module.

In case of a failure of any converter, the corresponding PV module of the PV string remains operative if that PV module is among the highly illuminated PV modules. Thus, the status of the PV string remains unchanged. The compensation power to all of the other lesser illuminated PV modules are supplied and the string current remains at its maximum corresponding to the highly illuminated PV modules. If any of the PV modules of the string is partially shaded, the string current is reduced due to the failure of the corresponding converter leading to graceful degradation. If the reduction in the string current is significant, the respective PV module is bypassed to allow the remaining PV string to operate normally. The operation of the PV string under this condition

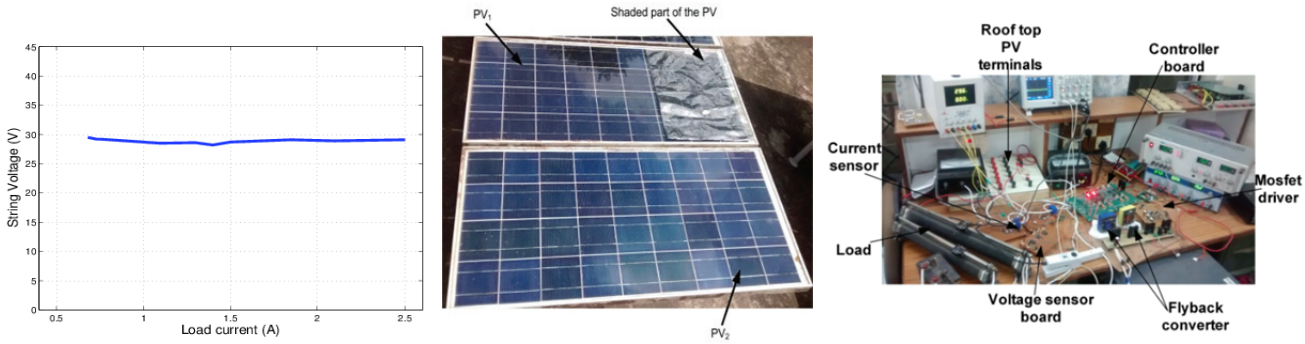

(a) (b) (c)

Fig. 20. (a) Load regulation; (b) PV modules used for the experiment; (c) Experimental setup.

TABLE V
COMPARISON OF PROPOSED SCHEME WITH EXISTING SCHEMES

Parameters	FPDC Scheme [13]-[15],[30]	CPDC Scheme [20]-[22]	Voltage Equalization Scheme [23]-[27]	Proposed Scheme
Power gain	Low ($P_g = P_T - P_{sw}$)	High	Medium ($P_g = P_T - P_{MPPT}$)	High
MPP Tracking efficiency	Exact MPP (99%)	Exact MPP (98.7%)	Approximate MPP (94%-96%)	High (99.4%)
Converter efficiency	96%	90%	92%	96.7%
Hardware burden	High	High	Low	Medium
No. of extra analog circuitry-	Nil	n	Nil	Nil
No. of current sensors-	n	n	1	n
No. of voltage sensors-	n	n	1	n
No.of switches-	n	2n+1	2n	n
Cost	High	Medium	Medium	Medium

is illustrated in Fig. 19(a), Fig. 19(b) and Fig. 19(c). In Fig. 19(a) both of the PV_1 and PV_2 modules are uniformly illuminated. Fig. 19(b) and Fig. 19(c) show the case in which PV_1 is unshaded and PV_2 is shaded. In Fig. 19(b), both of the converters are working normally. The string current is 1.36A, which corresponds to a highly illuminated PV module (PV_1) and both the PV modules operate at their respective MPPs. Fig. 19(c) shows a case in which the converter corresponding to PV_2 is faulty. The corresponding degradation in the string current is shown. The string current drops to 0.38A corresponding to the current of PV_2.

The regulation of the string voltage at a fixed radiation of 300W/m^2 for a variation in the load is shown in Fig. 20(a). The load is varied from 0.65A to 2.5A. The string voltage is regulated by the DPP units at their respective MPPs. The load regulation of the configuration is found to be 0.3%. A comparison of the extracted power from the experimental setup of the PV string with and without DPP units is listed in Table IV under two different cases. A prototype of the experimental setup is shown in Fig. 20(b) and Fig. 20(c).

A qualitative comparison of the RVP-DMPPT algorithm with existing DMPPT algorithms is presented in Table V. The cost of the scheme is evaluated based on the number of sensors and semiconductor devices used in the corresponding methods. The control complexity is evaluated based on the number of communication ports, the number of sampling instants sampling and the types of operations. In Table V, n is the number of PV modules/converters in the PV string. P_g is the effective power gain, P_T is total power generated by the string, P_{MPPT} is loss in power due to the approximate determination of the MPP, and P_{sw} is the converter switching loss.

IV. CONCLUSIONS

This paper presents an efficient RVP based DMPPT algorithm and a small signal model for the unidirectional DPP based PV-Bus architecture. The proposed RVP-DMPPT algorithm determines the exact MPP for each PV module under all atmospheric conditions with a high accuracy. The RVP-DMPPT algorithm does not require PV voltage sensing to compute power. This reduces both the control complexity and the computation time. The DMPPT algorithm reduces the hardware burden and exhibits a tracking efficiency of 99.4%. The dynamic behavior of the derived small signal model is verified with simulation and experimental results. The accuracy of the derived small signal model of the PV system is verified by demonstrating sudden changes in the irradiance.

REFERENCES

[1] S. Strache, R. Wunderlich, and S. Heinen, "A comprehensive, quantitative comparison of inverter architectures for various PV systems, PV cells, and irradiance profiles," *IEEE Trans. Sustain. Energy*, Vol. 5, No. 3, pp. 813-822, Jul. 2014.

[2] L. L. Villa, X. Pichon, F. S. Ardebili, B. Raison, J. Crebier, and A. Labonne, "Towards the design of control algorithms for a photovoltaic equalizer: Choosing the optimal switching strategy and the duty cycle," *IEEE Trans. Power Electron.*, Vol. 29, No. 3, pp. 1447-1460, Mar. 2014.

[3] I. R. Balasubramanian, S. I. Ganesan, and N. Chilakapati, "Impact of partial shading on the output power of PV systems under partial shading conditions," *IET Power Electron.*, Vol. 7, No. 3, pp. 657-666, Mar. 2014.

[4] S. Moballegh and J. Jiang, "Modeling, prediction, and experimental validations of power peaks of PV arrays under partial shading conditions." *IEEE Trans. Sustain. Energy*, Vol. 5, No. 1, pp. 293-300, Jan. 2014.

[5] C. Rahmann, V. Vittal, J. Ascui, and J. Haas, "Mitigation control against partial shading effects in large-scale PV power plants," *IEEE Trans. Sustain. Energy*, Vol. 7, No. 1, pp. 293-300, Jan. 2016.

[6] G. N. Psarros, E. I. Batzelis, and S. A. Papathanassiou, "Partial shading analysis of multistring PV arrays and derivation of simplified MPP expressions," *IEEE Trans. Sustain. Energy*, Vol. 6, No. 2, pp. 499-508, Apr. 2015.

[7] S. Lyden and Md. E. Haque, "A simulated annealing global maximum power point tracking approach for PV modules under partial shading conditions," *IEEE Trans. Power Electron.*, Vol. 31, No. 6, pp. 4171-4181, Jun. 2016.

[8] M. Boztepe, F. Guinjoan, G. Velasco-Quesada, S. Silvestre, A. Chouder, and E. Karatepe, "Global MPPT scheme for photovoltaic string inverters based on restricted voltage window search algorithm," *IEEE Trans. Industrial Electron.*, Vol. 61, No. 7, pp. 3302-3312, Jul. 2014.

[9] E. Koitroulis and F. Blaabjerg, "A new technique for tracking the global maximum power point of PV arrays operating under partial-shading conditions," *IEEE J. Photovoltaics*, Vol. 2, No. 2, pp. 184-190, Apr. 2012.

[10] X. Li, H. Wen, Y. Hu, L. Jiang, and W. Xiao, "Modified beta algorithm for GMPPT and partial shading detection in photovoltaic systems," *IEEE Trans. Power Electron.*, Vol. 33, No. 3, pp. 2172-2186, Mar. 2017.

[11] H. Patel and V. Agarwal, "MATLAB-based modeling to study the effects of partial shading on PV array characteristics," *IEEE Trans. Energy Convers.*, Vol. 23, No. 1, pp. 302-310, Mar. 2008.

[12] J. D. Bastidas-Rodriguez, E. Franco, G. Petrone, C. A. Ramos-Paja, and G. Spagnuolo, "Maximum power point tracking architectures for photovoltaic systems in mismatching conditions: A review," *IET Power Electron*, Vol. 7, No. 6, pp. 1396- 1413, Nov. 2014.

[13] F. Wang, R. Gou, T. Zhu, Y. Yang, and F. Zhuo, "Comparison of DMPPT PV system with different topologies," in *Proc. CICED*, pp. 1-5, Aug. 2016.

[14] C.-W. Chen and Y.-M. Chen, "Analysis of the series connected distributed maximum power point tracking PV system." in *Proc. APEC*, pp. 3083-3088, Mar. 2015.

[15] G. Petrone, G. Spagnuolo, and M. Vitelli, "An analog technique for distributed MPPT PV applications," *IEEE Trans. Ind. Electron.*, Vol. 59, No. 12, pp. 4713-4722, Dec. 2012.

[16] S. Sajadian and R. Ahmadi, "Distributed maximum power point tracking using model predictive control for photovoltaic energy harvesting architectures based on cascaded power optimizers," *IEEE J. Photovolt.*, Vol. 7, No. 3, pp. 849-857, May 2017.

[17] P. S. Shenoy, K. A. Kim, B. B. Johnson, and P. T. Krein, "Differential power processing for increased energy production and reliability of photovoltaic systems," *IEEE Trans. Power Electron.*, Vol. 28, No. 6, pp. 2968-2979, Jun. 2013.

[18] A. Diab-Marzouk and O. Trescases, "SiC-based bidirectional cuk converter with differential power processing and MPPT for a solar powered aircraft," *IEEE Trans. Transport. Electrific.*, Vol. 1, No. 4, pp. 369-381, Dec. 2015.

[19] Y.-T. Jeon, H. Lee, K. A. Kim, and J.-H. Park, "Least power point tracking method for photovoltaic differential power processing systems," *IEEE Trans. Power Electron.*, Vol. 32, No. 3, pp. 1941-1951, Mar. 2017.

[20] Y. Levron, D. R. Clement, B. Choi, C. Olalla, and D. Maksimovic, "Control of submodule integrated converters in the isolated-port differential power-processing photovoltaic architecture," *IEEE J. Emerg. Sel. Topics Power Electron.*, Vol. 2, No. 4, pp. 821-832, Dec. 2014.

[21] P. K. Peter, and V. Agarwal, "Current equalization in photovoltaic strings with module integrated ground-isolated switched capacitor DC-DC converters," *IEEE J. Photovolt.*, Vol. 4, No. 2, pp. 669-678, Mar. 2014.

[22] P. Sharma and V. Agarwal, "Maximum power extraction from a partially shaded PV array using shunt-series compensation" *IEEE J. Photovolt.*, Vol. 4, No. 4, pp. 1128-1137, Jul. 2014.

[23] P. Sharma and V. Agarwal, "Exact maximum power point tracking of grid-connected partially shaded PV source using current compensation concept," *IEEE Trans. Power Electron.*, Vol. 29, No. 6, pp. 4684-4692, Sep. 2014.

[24] G. R. Walker, J. Xue, and P. Sernia, "PV string per-module maximum power point enabling converters" in *Proc. Australasian Univ. Power Eng. Conf.*, pp. 112-117, 2003.

[25] G. R. Walker and P. C. Sernia, "Cascaded dc-dc converter connection of photovoltaic Modules," *IEEE Trans. Power Electron.*, Vol. 19, No. 4, pp. 1130-1139, Jul. 2004.

[26] T. Shimizu, M. Hirakata, T. Kamezawa, and H. Watanabe, "Generation control circuit for photovoltaic module," *IEEE Trans. Power Electron*., Vol.16, No.3, pp. 293-300, May 2001.

[27] M. Uno and A. Kukita, "Single-switch voltage equalizer using multistacked buck-boost converters for partially shaded photovoltaic modules," *IEEE Trans. Power Electron.*, Vol. 30, No. 6, pp. 3091-3105, Jun. 2015.

[28] M. Uno and A. Kukita, "Two-switch voltage equalizer using an LLC resonant inverter and voltage multiplier for partially shaded series-connected photovoltaic modules,"

IEEE Trans. Ind, Appl,, Vol. 51, No. 2, pp. 1587-1601, Apr. 2015.

[29] O. Khan, W. Xiao, and H. H. Zeineldin. "Gallium-nitride-based submodule integrated converters for high-efficiency distributed maximum power point tracking PV applications," *IEEE Trans. Ind. Electron.*, Vol. 63, No. 2, pp. 966-975, Feb. 2016.

[30] S. Strache, R. Wunderlich, and S. Heinen, "Maximum power point tracker for small number of solar cells connected in series," in *Proc. IECON*, pp. 5732-5737, Oct. 2012.

[31] F. Nicola, G. Lisi, G. Petrone, G. Spagnuolo, and M. Vitelli, "Distributed maximum power point tracking of photovoltaic arrays: Novel approach and system analysis," *IEEE Trans. Ind. Electron.*, Vol. 55, No. 7, pp. 2610-2621, Jul. 2008.

[32] C. Olalla, D. Clement, M. Rodriguez, and D. Maksimovic, "Architectures and control of submodule integrated DC-DC converters for photovoltaic applications," *IEEE Trans. Power Electron.*, Vol. 28, No. 6, pp. 2980-2997, Jun. 2013.

[33] R. W. Erickson and D. Maksimovic, *Fundamentals of Power Electronics*, Norwell, MA: Kluwer, 2001.

[34] Multi-crystalline PM045-055-36 series PV module datasheet, Photon Energy Systems Limited, Hyderabad, India, 2014.

Aniruddha Kamath M. received B.E. degree in Electrical and Electronics Engineering from the S.J. College of Engineering, Mysore, India, in 2005; and M.Tech. degree in Microelectronics and Control Systems from the NMAM Institute of Technology, Mangalore, India, in 2010. He is presently working towards his Ph.D. degree in Department of Electrical Engineering, National Institute of Technology Calicut, Kozhikode, India. He is presently working as Assistant Professor in the Canara Engineering College, Mangalore, India. His current research interests include PV power conversion systems, MPPT, DC/DC converters and AC/DC converters.

Jayanta Biswas received his B.E. degree in Computer Science from the Bengal Engineering College, Shibpur, Howrah, India, in 1993; and his M.E. and Ph.D. degrees in System Science and Automation from the Indian Institute of Science, Bengaluru, India, in 1995 and 2006, respectively. From January 1995 to 1998, he was with NCR Corporation, Columbia, SC, USA. From January 1999 to November 2002, he was with Alcatel Internetworking, Calabasas, CA, USA. From May 2000 to November 2002, he was the Project Manager of the Alcatel Internetworking ATM (core and edge) switch software development effort, and he was also leading the ten Gigabit software development effort. He worked as the Technical Director at CEM Solutions, Bangalore, India, where he was leading embedded product development and research activity as the Technical Director. He worked and taught as an Assistant Professor at the International Institute of Information Technology (IIIT), Bangalore, India, in the embedded systems and VLSI group. His current research interests include digital controller architectures for power management application ICs and modulation techniques for multilevel power electronics converters.

Anjana K. G. received the B.Tech. degree in Electrical and Electronics Engineering from the Govt. Engineering College, Thrissur, India, the M.Tech. degree in Power Electronics from National Institute of Technology, Kozhikode, India, in 2013. She is currently working towards the Ph.D. degree in Department of Electrical Engineering, National Institute of Technology Calicut, and Kozhikode, India. Her research interests include PV power conversion systems, MPPT and Pulse width modulated power electronic converters.

Mukti Barai received the B.E. degree in electrical engineering from Bengal Engineering College, Howrah, India, in 1992, and the M.Tech. and Ph.D. degrees in machine drives and power electronics from the Indian Institute of Technology, Kharagpur, India, in 1994 and 2009, respectively. From 1994 to 2000, she was a Senior Engineer (Design and Development) in the Electronics Division, Bharat Heavy Electricals Limited, Bangalore, India. From 2000 to 2002, she was a Principal Software Development Engineer at Alcatel Internetworking, Inc. From 2003 to 2004, she was at ST Microelectronics Research Laboratory, Indian Institute of Science, Bangalore. She is currently working as an Assistant Professor at the National Institute of Technology Calicut, Kozhikode, India.Her research interests include modulation techniques for multilevel power electronics converter and digital controller architectures for power management application ICs.